Arch. Mech., **63**, 5–6, pp. 573–598, Warszawa 2011

Local model of plane acoustic waves propagation in multilayered infinite sandwich structures

S. KARCZMARZYK

Institute of Machine Design Fundamentals
Warsaw University of Technology
Narbutta 84, 02-524 Warsaw, Poland
e-mail: karczmarzyk_st@poczta.onet.pl

A LOCAL MODEL FOR COMPUTING the coincidence frequencies and the transmission loss of multilayered infinite sandwich plates composed of isotropic layers is presented in the paper. The model is derived within the local theory of linear elastodynamics under assumption that only one component of the vector potential is equivalent to zero and after application of the Pythagorean theorem. Any simplifications concerning the structure have not been introduced. A passage from the acoustic model to some plate benchmark models is shown. Numerical results predicted by the model for homogeneous, three-layer sandwich and five-layer sandwich infinite-infinite plates are obtained and compared with the results predicted by other models existing in the literature. Both flexural and breathing waves are numerically analysed. Some conclusions of practical importance have also been formulated.

Key words: acoustic waves, linear elastodynamics, multilayered plate, local model, coincidence frequencies, transmission loss.

Notations

c	sound velocity in the air,
c_s	phase velocity in the structure,
E, $E_{(j)}$	Young's modulus and Young's modulus of j-th layer, respectively,
$f_c = \omega_c/2\pi$	coincidence frequency,
$f_{\rm cr} = \omega_{cr}/2\pi$	critical coincidence frequency,
$h_{(j)}$	thickness of j-th layer of the plate,
k	wave number of the acoustic wave,
k_s	wave number of the wave propagating in the structure,
k_x, k_y	wave number components in directions x and y, respectively,
u_x, u_y, u_z	displacements in directions x, y, z, respectively,
$u_{1(j)}$, $u_{2(j)}$, $u_{3(j)}$	displacements within j-th layer in directions 1, 2, 3, respectively,
t	time,
x, y, z	space variables,
$Z_{\rm air}$	impedance of the air,
ε_{qr}	strain tensor,
θ	incident angle of the plane wave,

λ, μ Lamé's parameters,
μ, $\mu_{(j)}$ shear modulus and shear modulus of j-th layer, respectively,
ν, $\nu_{(j)}$ Poisson's ratio and Poisson's ratio of j-th layer, respectively,
ρ, $\rho_{(j)}$ density and density of j-th layer, respectively,
ρ_{air} density of the air,
$\sigma_{zz(j)}$ normal stress in j-th layer,
$\sigma_{33}(j)$, $\sigma_{31(j)}$, $\sigma_{23(j)}$ normal and shear stresses in j-th layer, respectively,
ω frequency,
$\omega_c = 2\pi f_c$ coincidence frequency,
$\omega_{\text{cr}} = 2\pi f_{cr}$ critical coincidence frequency,

$$\nabla^2 = \frac{\partial^2}{\partial x_1^2} + \frac{\partial^2}{\partial x_2^2} + \frac{\partial^2}{\partial x_3^2}.$$

1. Introduction

NOWADAYS A PROTECTION OF PEOPLE AGAINST NOISE and vibration is one of the most important tasks for designers of machines and buildings [1, 2]. There are many ways to do it and one of them is application of layered structural elements as the sound-insulating members in engineering structures. In particular, multi-layered panels composed of alternately arranged thin stiff layers and soft thick layers are most promising for the insulation purposes. Therefore, among other things, the three-layer sandwich panels are embedded in trains structures [3], in ships hulls [4], in airplanes fuselages [5], while multi-layer boards are applied in buildings engineering [6].

A reasonable application of the layered structural elements for sound insulation in a particular case may require using both the experimental and simulation methods to define design charts, that is to evaluate in the domain of frequency such parameters as the sound transmission loss (TL) or the sound insertion loss (IL) for the structure. One may say that evaluating of the TL and the IL in domain of frequency are the main tasks of any sound insulation theory (model).

The plane layered and homogeneous sound insulationg structural elements can be divided into three groups: (1) infinite-infinite (I-I) panels that is very large, comparing with the acoustic wave(s) length(s), in two perpendicular directions x, y – see Fig. 1, (2) finite-infinite (F-I) elements such as covers of ducts and (3) finite-finite, in the directions x, y, (F-F) plates. The above division of the structures is used in the further text to comment the references.

A Reader may find easily in the literature a detailed analysis of the sound insulation problems mainly for the I-I homogeneous panels, and for multiple homogeneous I-I panels, with gaps between them filled with the air or with porous materials [6]. The analysis is obtained within the classical theory of homogeneous plate based on the hypothesis of plane cross-sections, and for an assumed plane incident wave(s) of infinite extent. The analysis is known as the one-dimensional sound insulation theory.

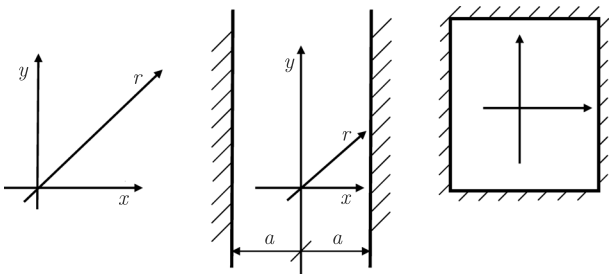

FIG. 1. Three groups of plane sound insulating elements, I-I panel, F-I element and F-F plate, respectively.

In [7], combining of the one-dimensional theory for the homogeneous panel with a single layer theory of sandwich panel was proposed to obtain a sound insulation model for the sandwich I-I structure. More refined model which can be applicable to the acoustic analysis of the sandwich structures was developed in [8]. It was used by the Authors to obtain the dispersion curves and to define the waves propagating and evanescent in the I-I sandwich structure. A refined approach to modeling of acoustic phenomena occuring in sandwich I-I panels was presented in [9, 10]. This model was derived by combining the equation of motion of the classical plate theory, based on the plane cross-sections, and the linear elastodynamics (Lamé) equations of motion, while the first one is satisfied within the outer layers of the sandwich panel and the latter are satisfied within the middle layer (core) of the structure. It is noted that the mixed model [9, 10] predicts within the core both the flexural 'in-phase' wave motions and the breathing 'anti-phase' wave motions – not predicted by models [7, 8]. The compatibility equations of displacements and stresses in the interfaces have also been fulfilled in the mixed model. The authors compared the mixed model with some models existing in the literature by means of the dispersion curves and investigated some properties of the I-I structure [9, 10].

The TL curves in domain of frequency for F-F sandwich three-layer plates, as well as the mathematical model of sound insulation, were obtained in papers [11, 12]. In particular, the explicit expression for the TL of the F-F plate is given and an influence of the material coupling on the TL curve is analysed in [11, 12].

Another model for computations of the TL factor of the three-layer sandwich panel was presented in [13] and it also predicts both the 'in-phase' and 'anti-phase' wave motions in the core. The authors computed, according to the model, the TL curves in the domain of frequency for four F-F sandwich panels and compared the computational results with measured data published in [14]. It is noted that to compute the TL curves for the F-F sandwich plates, considered in [13], some formulas derived from a simpler model, printed in [15], were used. Paper [16] contains similar information, obtained both numerically and exper-

imentally, about the sound insulation properties of the F-F sandwich plate as in [13]. Additionally, a comparison of the TL for sandwich I-I and F-F panels is presented in [16]. Upon basis of the data one can say that for frequencies higher than the lowest coincidence frequency, the TL of the I-I structure is much higher than the parameter measured for one of the F-F simply supported sandwich plates investigated in [16].

In order to obtain, for a particular structure, a valuable TL curve in domain of frequency, one should first evaluate the coincidence frequencies. For a purely elastic I-I or F-F structure, that is for the structures with negligible internal damping of the wave motions, the TL is equal to zero at the critical coincidence frequency and it is very small in vicinity of the other coincindence frequencies. Therefore, evaluation of the coincidence frequencies should be the first step within the sound insulation procedure.

In [17] the Reader will find important considerations on the coincidence frequencies of the F-F homogeneous plate. The authors have been formulated conditions for existing of many coincidence frequencies in the F-F plate. It has also been stated in [17] that the lowest coincidence frequency, called critical coincidence frequency, of the F-F plate equals the critical coincidence frequency for the I-I panel with the same cross-sectional parameters as the F-F plate. Since the critical coincidence frequency is the only one at which the TL of a F-F plate equals zero (see [17]), then its evaluation is the fundamental task within the sound insualtion procedure. Let us note finally that due to the property stated above, the critical coincidence frequency can be calculated either within models (theories) for the F-F plates or within the corresponding models for the I-I panels.

In [18] the Reader will find considerations on the critical coincidence frequencies of plane homogeneous and layered I-I panels. The analysis in [18] is done by using equations of motion derived within the classical plate theory, Mindlin's type plate theory and within a thin plate theory by Jones [19]. Unfortunately, the equations of motion for the thick structures, applied in paper [18], are unstable since for the plane wave motion they imply imaginary angular frequency of the wave. The problem is not discussed here more widely and the Reader interested in its analysis is encouraged to aquaint with [20] Sections 4 and 6, where it is discussed in an original way. The coincidence frequencies of the three-layer sandwich I-I structures are analysed numerically in [21]. It was shown in [21], among other things, that the coincidence frequency increases when the shear modulus of the middle layer of the sandwich panel decreases.

The short analysis of the recently published papers (see the references), shows the following deficiences of the models and investigations: (1) all the models outlined above are not directly applicable to the acoustic analysis of the multilayered (e.g., five-layers, seven-layers etc.) sandwich structures which are the most

promising as the sound insulating members, (2) some of the published models are not capable of predicting the breathing modes of the wave motions which may occur in the sandwich structures with thick and soft layers and (3) some of the existing models are not stable in the sense pointed out in [20]. The deficiences (1)–(3) do not occur in the local model proposed in the present paper.

Details of the local model are presented in the subsequent sections of the paper, however it is noted here that the model is applicable to layered structures composed of any numbers of layers of different materials (phases), thicknesses and stiffnesses. Therefore, this model is not similar to the family of continuum models applicable to the slowly graded laminates (SGL) – see e.g. [22]. The continuum models, including [22], are based on many refined assumptions enabling both inclusion of the cross-sectional inhomogeneity of the SGLs and a relative simplicity of the the models, despite their applicability to the SGLs consisting of a large number of layers.

This paper is structured as follows. In Section 2, a statement of the problem is outlined. In Section 3, an exact solution to the wave equations of the local theory of linear elastodynamics is derived under assumption that one function of the vector potential is equivalent to zero. In Section 4 a transformation and reduction of the solution to the well-known 2D form is shown. In Section 5, some details on the boundary conditions and numerical aspects of the problem are presented. In Section 6, numerical results predicted by the local model are presented, compared and/or discussed. Section 7 contains some conclusions. In Appendices A and B, some basic information on the coincidence phenomenon and on the transmission loss are presented.

2. Statement of the problem

The structure considered here is composed of p isotropic layers. It is infinite in directions x, y and its thickness h, being the sum of thicknesses of the layers, extends in direction z – see Fig. 2.

It is well-known due to Lamé [23, 24] that the displacement field $\mathbf{u}$ (see Notations) which is defined, for each j-th idividual layer separately, as follows:

$$\begin{aligned} &\mathbf{u} = \operatorname{grad}\phi + \operatorname{rot}\boldsymbol{\psi} \equiv u_k = \phi_{,k} + e_{klm}\psi_{m,l}, \\ &\mathbf{u} = \{u_1\ u_2\ u_3\}, \qquad k,l,m = 1,2,3, \end{aligned} \tag{2.1}$$

satisfies the local equations of motion of the linear elastodynamics within the j-th layer, provided that the functions ϕ and ψ_k satisfy the following wave equations

$$[(\lambda+2\mu)/\rho]\nabla^2\phi - \frac{\partial^2\phi}{\partial t^2} = 0, \qquad (\mu/\rho)\nabla^2\psi_m - \frac{\partial^2\psi_m}{\partial t^2} = 0, \qquad m = 1,2,3, \tag{2.2}$$

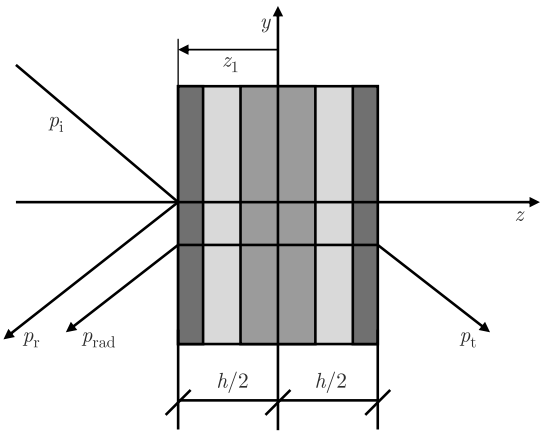

FIG. 2. Cross-section of the structure and pressures: p_i – incident, p_r – reflected, p_rad – radiated, p_t – transmitted.

and functions ψ_k satisy additionally

$$\psi_{k,k} \equiv \psi_{1,1} + \psi_{2,2} + \psi_{3,3} = 0. \tag{2.3}$$

It is noted that displacements (2.1) satisfy both the wave equations (2.2) and the well known Saint–Venant compatibility equations (originally expressed in terms of the strains) within each j-th layer separately, $j = 1, 2, \ldots, p$. For a particular j-th layer, the Lamé parameters λ, μ and density ρ, appearing in the wave equations (2.2), should be replaced with $\lambda_{(j)}$, $\mu_{(j)}$ and $\rho_{(j)}$, respectively.

The following through-the-thickness boundary conditions for a plate have to be satisfied,

$$\begin{aligned} &\sigma_{33}(x, y, z = z_r) \equiv \sigma_{zz}(x, y, z = z_r) = q_r, \\ &\sigma_{31}(x, y, z = z_r) \equiv \sigma_{zx}(x, y, z = z_r) = 0, \\ &\sigma_{32}(x, y, z = z_r) \equiv \sigma_{yz}(x, y, z = z_r) = 0, \end{aligned} \tag{2.4}$$

where q_r denotes the normal acoustic loading acting on the surface, whereas subscript $r = 1, 2$. If we assume that the substript r equals 1 ($q_r = q_1$) for the top/left outisde surface of the plate, then r equals 2 ($q_r = q_2$) for the bottom/right outside surface of the plate, respectively. Symbol z_r in (2.4) denotes coordinates of the outside surfaces of the multilayered panel – see Fig. 2.

Between adjoining layers of the plate, with subscripts j and $j+1$, the following local compatibility equations for the normal and shear stresses as well as for the in-plane and out-of-plane displacements, are satisfied,

$$\begin{aligned} &\sigma_{33(j)} = \sigma_{33(j+1)}, \quad \sigma_{31(j)} = \sigma_{31(j+1)}, \quad \sigma_{23(j)} = \sigma_{23(j+1)}, \\ &u_{1(j)} = u_{1(j+1)}, \quad u_{2(j)} = u_{2(j+1)}, \quad u_{3(j)} = u_{3(j+1)}. \end{aligned} \tag{2.5}$$

It is finally summarized that statement of the problem contains the following equations: the kinematic assumptions (2.1) – satisfied individually for each layer, the wave equations (2.2) – satisfied individually for each layer, the Saint–Venant compatibility equations – satisfied individually for each layer, the calibration condition (2.3) – satisfied individually for each layer, the boundary conditions (2.4) – for the (outside) surfaces of the structure, the compatibility equations (2.5) between adjoining layers and the constitutive equation (the Hooke's law) – satisfied individually for each layer.

3. Derivation and analysis of a solution to the wave equations

In this section the solution, derived in an original way by the present author, is presented. The solution is obtained under assumption that one of the functions ψ_k occurring in the general Lamé solution (2.1) is equivalent to zero. In fourth section the solution is transformed to the well-known, frequently presented the literature, 2D solution applicable entirely to the I-I plates. Taking into consideration (2.1) one may write the displacements in the extended form:

$$\begin{aligned} u_1 &\equiv u_x = \phi_{,x} - \psi_{2,z} + \psi_{3,y} = u_{x1} + u_{x2}, \\ u_2 &\equiv u_y = \phi_{,y} - \psi_{3,x} + \psi_{1,z} = u_{y1} + u_{y2}, \\ u_3 &\equiv u_z = \phi_{,z} - \psi_{1,y} + \psi_{2,x} = u_{z1} + u_{z2}. \end{aligned} \tag{3.1}$$

The following nomenclature is applied in Eqs. (3.1):

$$\begin{aligned} u_{x1} &= -\psi_{2,z} + \psi_{3,y}, \qquad u_{x2} = \phi_{,x}, \\ u_{y1} &= -\psi_{3,x} + \psi_{1,z}, \qquad u_{y2} = \phi_{,y}, \\ u_{z1} &= -\psi_{1,y} + \psi_{2,x}, \qquad u_{z2} = \phi_{,z}. \end{aligned} \tag{3.2}$$

It is noticed that

$$u_{x1,x} + u_{y1,y} + u_{z1,z} \equiv 0, \qquad u_{x2,x} + u_{y2,y} + u_{z2,z} = \nabla^2 \phi. \tag{3.3}$$

The problem considered here can be solved for the following, simplifying assumption:

$$\psi_3 \equiv 0. \tag{3.4}$$

The displacements are now as follows,

$$\begin{aligned} u_{x1} &= -\psi_{2,z}, & u_{x2} &= \phi_{,x}, \\ u_{y1} &= +\psi_{1,z}, & u_{y2} &= \phi_{,y}, \\ u_{z1} &= -\psi_{1,y} + \psi_{2,x}, & u_{z2} &= \phi_{,z}. \end{aligned} \tag{3.5}$$

We further assume that ψ_n are the plane waves, i.e.,

$$\psi_n = X_n(x)Y_n(y)\tilde{Z}_n(z)T(t) = \tilde{Z}_n(z)e^{i(\omega t - k_x x - k_y y)}, \quad i^2 = -1,\ n = 1, 2, \tag{3.6}$$

where the functions of variable z are unknown, k_x and k_y denote the wave numbers in directions x and y, respectively, and ω stands for the wave frequency.

After substituting (3.6) into (2.3) one obtains

$$\tilde{Z}_2(z) = -(k_x/k_y)\tilde{Z}_1(z), \tag{3.7}$$

$$\begin{aligned} u_{x1} &= -\psi_{2,z} = (k_x/k_y)\tilde{Z}_{1,z}e^{i(\omega t - k_x x - k_y y)}, \\ u_{y1} &= +\psi_{1,z} = \tilde{Z}_{1,z}e^{i(\omega t - k_x x - k_y y)}, \\ u_{z1} &= -\psi_{1,y} + \psi_{2,x} = i[(k_x^2 + k_y^2)/k_y]\tilde{Z}_1(z)e^{i(\omega t - k_x x - k_y y)}). \end{aligned} \tag{3.8}$$

If we introduce the following notation:

$$Z_{1,z} = \tilde{Z}_{1,z}/k_y, \tag{3.9}$$

the displacements (3.8) will be in the form:

$$\begin{aligned} u_{x1} &= k_x Z_{1,z}e^{i(\omega t - k_x x - k_y y)} = iZ_{1,z}(-ik_x)e^{i(\omega t - k_x x - k_y y)}, \\ u_{y1} &= k_y Z_{1,z}e^{i(\omega t - k_x x - k_y y)} = iZ_{1,z}(-ik_y)e^{i(\omega t - k_x x - k_y y)}, \\ u_{z1} &= i(k_x^2 + k_y^2)Z_1(z)e^{i(\omega t - k_x x - k_y y)}). \end{aligned} \tag{3.10}$$

Taking into consideration (3.5) and (3.10) one obtains,

$$\psi_1 = +iZ_1(-ik_y)e^{i(\omega t - k_x x - k_y y)}, \qquad \psi_2 = -iZ_1(-ik_x)e^{i(\omega t - k_x x - k_y y)}. \tag{3.11}$$

Let us note finally that the wave equations (2.2), containing functions ψ_n, where now $n = 1, 2$, imply the following equation for the function Z_1,

$$(\mu/\rho)\nabla^2\psi_n + \frac{\partial^2\psi_n}{\partial t^2} = 0 \equiv Z_{1,zz} - (k_x^2 + k_y^2 - \rho\omega^2/\mu)Z_1 = 0, \tag{3.12}$$

and the following expressions for the shear stresses:

$$\begin{aligned} \sigma_{zx1} &= \mu[iZ_{1,zz} + (k_x^2 + k_y^2)iZ_1](-ik_x)e^{i(\omega t - k_x x - k_y y)} \\ &= \mu[2(k_x^2 + k_y^2) - \rho\omega^2/\mu]Z_1 k_x e^{i(\omega t - k_x x - k_y y)}, \\ \sigma_{yz1} &= \mu[iZ_{1,zz} + (k_x^2 + k_y^2)iZ_1](-ik_y)e^{i(\omega t - k_x x - k_y y)} \\ &= \mu[2(k_x^2 + k_y^2) - \rho\omega^2/\mu]Z_1 k_y e^{i(\omega t - k_x x - k_y y)}. \end{aligned} \tag{3.13}$$

The solution derived in this section is composed of two (not of three) Lamé's rotational functions. As far as the author knows it is not common in the literature. It is noted that to obtain the displacements u_{x2}, u_{y2}, u_{z2}, appearing in (3.1), (3.2), one needs to derive the function ϕ. Assuming that ϕ is in the form expressed in (3.6), it can be derived from the left-hand side Eq. (2.2) .

$$\phi = X_n(x)Y_n(y)(z)T(t) = \tilde{\Phi}(z)e^{i(\omega t - k_x x - k_y y)}, \qquad i^2 = -1, \tag{3.14}$$

$$[(\lambda + 2\mu)/\rho]\nabla^2\phi - \frac{\partial^2\phi}{\partial t^2} = 0 \equiv \tilde{\Phi}_{,zz} - [k_x^2 + k_y^2 - \rho\omega^2/(\lambda + 2\mu)]\tilde{\Phi} = 0, \tag{3.15}$$

$$\begin{aligned} u_{x2} &= \phi_{,x} = -ik_x\tilde{\Phi}(z)e^{i(\omega t - k_x x - k_y y)}, \\ u_{y2} &= \phi_{,y} = -ik_y\tilde{\Phi}(z)e^{i(\omega t - k_x x - k_y y)}, \\ u_{z2} &= \phi_{,z} = \tilde{\Phi}_{,z}(z)e^{i(\omega t - k_x x - k_y y)}). \end{aligned} \tag{3.16}$$

After obtaining the displacements u_{x2}, u_{y2}, u_{z2}, the corresponding stresses must be obtained following the standard way. The shear stresses are defined as follows:

$$\begin{aligned} \sigma_{zx2} &= -2\mu ik_x\tilde{\Phi}_{,z}e^{i(\omega t - k_x x - k_y y)}, \\ \sigma_{yz2} &= -2\mu ik_y\tilde{\Phi}_{,z}e^{i(\omega t - k_x x - k_y y)}. \end{aligned} \tag{3.17}$$

The total displacements are composed of (3.1), (3.10) and (3.16),

(3.18)

$$\begin{aligned} u_x &= [iZ_{1,z} + \tilde{\Phi}(z)](-ik_x)e^{i(\omega t - k_x x - k_y y)} = [iZ_{1,z} + \tilde{\Phi}(z)]\frac{\partial e^{i(\omega t - k_x x - k_y y)}}{\partial x}, \\ u_y &= [iZ_{1,z} + \tilde{\Phi}(z)](-ik_y)e^{i(\omega t - k_x x - k_y y)} = [iZ_{1,z} + \tilde{\Phi}(z)]\frac{\partial e^{i(\omega t - k_x x - k_y y)}}{\partial y}, \\ u_z &= [i(k_x^2 + k_y^2)Z_1(z) + \tilde{\Phi}_{,z}]e^{i(\omega t - k_x x - k_y y)}). \end{aligned}$$

The total shear stresses in directions x, y are as follows:

$$\begin{aligned} \sigma_{zx1} &= \mu[iZ_{1,zz} + (k_x^2 + k_y^2)iZ_1 + 2\tilde{\Phi}_{,z}](-ik_x)e^{i(\omega t - k_x x - k_y y)}, \\ \sigma_{yz1} &= \mu[iZ_{1,zz} + (k_x^2 + k_y^2)iZ_1 + 2\tilde{\Phi}_{,z}](-ik_y)e^{i(\omega t - k_x x - k_y y)}. \end{aligned} \tag{3.19}$$

The total normal stress perpendicular to the interfaces of the structure is

$$\begin{aligned} \sigma_{zz} = 2\mu(k_x^2 + k_y^2)iZ_1, ze^{i(\omega t - k_x x - k_y y)}) \\ + [2\mu(k_x^2 + k_y^2) - \rho\omega^2]\tilde{\Phi}(z)e^{i(\omega t - k_x x - k_y y)}. \end{aligned} \tag{3.20}$$

The displacements can be expressed in the same form as the benchmark kinematic model applied in [25] and in many other papers. Namely, if the following nomenclature is introduced,

$$g(z) = -iZ_{1,z}, \qquad f(z) = i(k_x^2 + k_y^2)Z_1(z), \tag{3.21}$$

one can transform displacements (3.10) to the form appearing in [25]:

$$\begin{aligned} u_{x1} &= -g(z)Y(y)dX/dx e^{i\omega t}, \\ u_{y1} &= -g(z)dY/dy X(x)e^{i\omega t}, \\ u_{z1} &= f(z)Y(y)X(x)e^{i\omega t}. \end{aligned} \tag{3.22}$$

The same can be done for the displacements (3.16).

4. Reduction of ingredients of the in-plane displacements and stresses for an I-I structure – transformation of the above solution to a 2D form

It is seen from Eqs. (3.10), (3.13), (3.16) and (3.17) that

$$u_{x1}/u_{y1} = \sigma_{zx1}/\sigma_{yz1} = u_{x2}/u_{y2} = \sigma_{zx2}/\sigma_{yz2} = k_x/k_y. \tag{4.1}$$

Due to (4.1) we can reduce the above solution to the wave equations (2.2) to a 2D form. This means replacement of the displacements u_{x1}, u_{y1} and u_{x2}, u_{y2} as well as the shear stresses σ_{zx1}, σ_{yz1} and σ_{zx2}, σ_{yz2} by the following equivalent counterparts:

$$\begin{aligned} u_{r1} &= \sqrt{u_{x1}^2 + u_{y1}^2} = -i\sqrt{k_x^2 + k_y^2}iZ_{1,z}e^{i(\omega t - k_x x - k_y y)}, \\ u_{r2} &= \sqrt{u_{x2}^2 + u_{y2}^2} = -i\sqrt{k_x^2 + k_y^2}\tilde{\Phi}(z)e^{i(\omega t - k_x x - k_y y)}, \end{aligned} \tag{4.2}$$

$$\begin{aligned} \sigma_{zr1} &= \sqrt{\sigma_{zx1}^2 + \sigma_{yz1}^2} \\ &= -\mu i\sqrt{k_x^2 + k_y^2}[iZ_{1,zz} + (k_x^2 + k_y^2)iZ_1]e^{i(\omega t - k_x x - k_y y)}, \end{aligned} \tag{4.3}$$

$$\sigma_{zr2} = \sqrt{\sigma_{zx2}^2 + \sigma_{yz2}^2} = -2\mu i\sqrt{k_x^2 + k_y^2}\tilde{\Phi}_{,z}e^{i(\omega t - k_x x - k_y y)}.$$

Let the k_x and k_y be defined as follows:

$$k_x = k\sin\theta\cos\beta, \qquad k_y = k\sin\theta\sin\beta, \qquad k_x^2 + k_y^2 = k^2\sin^2\theta, \tag{4.4}$$

while θ denotes the incident angle of the wave and β is the angle between the directions x, r defined as follows (see Fig. 1):

$$\cos\beta = x/r = x/\sqrt{x^2+y^2}, \qquad \sin\beta = y/r = y/\sqrt{x^2+y^2}. \tag{4.5}$$

Due to (4.2)–(4.5), the in-plane displacements u_{r1}, u_{r2}, u_r and the shear stresses σ_{zr1}, σ_{zr2} and σ_{zr}in the infinite plate are defined as follows:

$$\begin{aligned} u_{r1} &= +k\sin\theta Z_{1,z} e^{i(\omega t - k\sin\theta r)}, \\ u_{r2} &= -ik\sin\theta\tilde{\Phi}(z) e^{i(\omega t - k\sin\theta r)}, \end{aligned} \tag{4.6}$$

$$u_r = u_{r1} + u_{r2} = -ik\sin\theta[iZ_{1,z} + \tilde{\Phi}(z)]e^{i(\omega t - k\sin\theta r)}, \tag{4.7}$$

$$\begin{aligned} \sigma_{zr1} &= \mu k\sin\theta(2k^2\sin^2\theta - \rho\omega^2/\mu)Z_1 e^{i(\omega t - k\sin\theta r)}, \\ \sigma_{zr2} &= -2\mu ik\sin\theta\tilde{\Phi}_{,z} e^{i(\omega t - k\sin\theta r)}, \end{aligned} \tag{4.8}$$

$$\begin{aligned} \sigma_{zr} &= \sigma_{zr1} + \sigma_{zr2} \\ &= -\mu ik\sin\theta[(2k^2\sin^2\theta - \rho\omega^2/\mu)iZ_1 + 2\tilde{\Phi}_{,z}]e^{i(\omega t - k\sin\theta r)}. \end{aligned} \tag{4.9}$$

It is seen from (4.7) and (4.9) that for $\theta = 0$, the in-plane wave motions and the corresponding shear stresses are equal to zero. Apart from the in-plane displacement u_r and the shear stress σ_{zr} in direction r, the acoustic plane wave induces in the infinite plate the out-of-plane displacement u_z and the stress σ_{zz}, defined by (3.18) and (3.20), respectively. The relationships can be expressed finally as follows:

$$\begin{aligned} u_z &= [ik^2\sin^2\theta Z_1(z) + \tilde{\Phi}_{,z}]e^{i(\omega t - k\sin\theta r)}), \\ \sigma_{zz} &= 2\mu k^2\sin^2\theta i Z_1, z e^{i(\omega t - k\sin\theta r)}) \\ &\quad + [2\mu k^2\sin^2\theta - \rho\omega^2]\tilde{\Phi}(z) e^{i(\omega t - k\sin\theta r)}. \end{aligned} \tag{4.10}$$

The expressions (4.7), (4.9) and (4.10), useful for obtaining final forms of the problems considered in the paper, have been derived under assumption that one function of the vector potential is equivalent to zero after applying the Pythagorean theorem. As far as the author knows, the approach is not common in the literature.

To complete the analysis we should say that the 2D displacement field (4.7), (4.10) can be obtained following another way, under the following assumptions:

$$u_y = u_{y1} + u_{y2} = 0, \quad \psi_1 = \psi_3 \equiv 0, \quad \psi_2 = \psi_2(x,z,t), \quad \phi = \phi(x,z,t). \tag{4.11}$$

As a consequence of (4.11) we obtain directly from (3.2) the following relationships:

$$u_{x1} = -\psi_{2,z}, \qquad u_{x2} = \phi_{,x}, \qquad u_{z1} = +\psi_{2,x}, \qquad u_{z2} = \phi_{,z}. \tag{4.12}$$

The way to obtain the 2D solution starting from the assumptions (4.11) is very popular in the literature, e.g., it is applied in [9, 10].

5. Some details on through-the-thickness boundary conditions

The surface pressures must be equated to the normal stresses on the outer sides of the structure – see Eqs. (2.4). When the plate is composed of p layers, the boundary conditions are as follows:

$$\sigma_{zz(1)}(x,y,z=z_1)=q_1, \qquad \sigma_{zz(p)}(x,y,z=z_1+h)=q_2, \qquad h=\sum_{1}^{p} h_{(j)}. \tag{5.1}$$

Symbol z_1 in (5.1) denotes coordinate of the outside surface of the first layer of the multilayered panel – see Fig. 2. The normal stresses appearing in (2.4) and (5.1) contain both the component resulting from the wave motions u_{x1}, u_{y1}, u_{z1} and the ingredient resulting from the wave motions u_{x2}, u_{y2}, u_{z2} – appearing in (3.1)–(3.3) and (3.5). The same refers to the shear stresses. Let us note that in the case of I-I panel there are no other boundary conditions than (2.4) and (5.1).

The loadings q_1, q_2 are defined as follows:

$$q_1=Z_{\text{air}}\frac{\partial u_z(z=-h/2)}{\partial t}, \qquad q_2=Z_{\text{air}}\frac{\partial u_z(z=+h/2)}{\partial t}, \qquad Z_{\text{air}}=\rho_{\text{air}}c. \tag{5.2}$$

They result from the partial pressures shown in Fig. 2. For the I-I structure, the partial pressures and the total loadings are defined as follows [7, 11],

$$\begin{aligned} p_i &= A_i e^{i(\omega t-k_x x-k_y y+k_z h/2)}, & p_r &= A_r e^{i(\omega t-k_x x-k_y y-k_z h/2)},\\ p_{\text{rad}} &= A_{\text{rad}} e^{i(\omega t-k_x x-k_y y-k_z h/2)}, & p_t &= A_t e^{i(\omega t-k_x x-k_y y-k_z h/2)}. \end{aligned} \tag{5.3}$$

If the origin of the coordinate system is moved to the surface loaded by the incident acoustic wave, the new space variable $z_1=z+h/2$ will appear in (5.1)–(5.3) and the above pressures will be defined as follows:

$$\begin{aligned} p_i &= A_i e^{i(\omega t-k_x x-k_y y)}, & p_r &= A_r e^{i(\omega t-k_x x-k_y y)},\\ p_{\text{rad}} &= A_{\text{rad}} e^{i(\omega t-k_x x-k_y y)}, & p_t &= A_t e^{i(\omega t-k_x x-k_y y-k_z h)}. \end{aligned} \tag{5.4}$$

Due to (5.4) the total acoustic loadings of the structure can be expressed in the way [13]:

$$\begin{aligned} q_1 &= p_i+p_r+p_{\text{rad}}=2p_i+p_{\text{rad}}=2p_i-Z_{\text{air}}\frac{\partial u_z(x,y,z_1=0,t)}{\partial t},\\ q_2 &= p_t=+Z_{\text{air}}\frac{\partial u_z(x,y,z_1=+h,t)}{\partial t}. \end{aligned} \tag{5.5}$$

Relationship (5.5) for q_1 is obtained under the assumption that $A_i = A_r$ – used in [7, 13]. Directly from (5.2) and (5.5) one obtains,

$$p_{\text{rad}} = -Z_{\text{air}}\dot{u}_z(x, y, z_1 = 0, t), \qquad p_t = +Z_{\text{air}}\dot{u}_z(x, y, z_1 = +h, t). \tag{5.6}$$

The total displacements and stresses resulting from the shear waves induced and propagating in the structure consist of two parts, one symmetric with respect to the space variable z and the latter antisymmetric with respect to z. Therefore, we can write the following expressions:

$$\frac{\partial u_z}{\partial t} = \frac{\partial u_{zs}}{\partial t} + \frac{\partial u_{za}}{\partial t}, \qquad \sigma_{zr} = \sigma_{zrs} + \sigma_{zra}, \qquad \sigma_{zz} = \sigma_{zza} + \sigma_{zzs}. \tag{5.7}$$

The properties of the displacements and stresses expressed in (5.7) may be explored to obtain the final (numerical) form of the boundary problem. In particular, for the structure symmetric about its middle plane, the problem can be splited into two subproblems: the flexural problem and the breathing one. Taking into consideration Eqs. (2.4), (2.5), (5.1)–(5.5) one can show that to compute the coincidence frequencies one has to solve numerically an eigenvalue transcendental problem, and to compute the TL one has to solve numerically a nonhomogeneous problem.

The eigenvalue transcendental problem is of the form $\det(\mathbf{A}) = F(\omega, k_s(\omega)) = 0$, where $\mathbf{A}$ denotes the square matrix of the boundary problem, here obtainable after satisfying all through-the-thickness boundary and compatibility conditions, i.e. Eqs (2.4), (2.5). The function $k_s(\omega)$ denotes dependence of the wavenumber on frequency for the structure considered. It is called 'dispersion curve' in the literature and it is unknown.

In fact, the above transcendental eigenvalue problem splits into two subproblems. When we assume $k_s = (\omega/c)\sin\theta$, then equation $\det(\mathbf{A}) = 0$ enables us to compute the coincidence frequencies (see also the Appendix A). After assuming that $\omega = \omega_g$, where ω_g is a given (assumed) value of frequency, the equation $\det(\mathbf{A}) = F(\omega_g, k_s(\omega_g)) = 0$, so-called dispersion equation, enables us to compute the wavenumber(s) and finally, for a series of the assumed frequencies, to obtain the dispersion curve(s).

For a particular boundary problem the transcendental equation implies infinite number of the coincidence frequencies: $\omega_{c1}, \omega_{c2}, \omega_{c3}, \ldots$ as well as the dispersion curves $k_{s1}, k_{s2}, k_{s3}, \ldots$. Usually, a finite number of the coincidence frequencies and dispersion curves is of practical importance and numerically obtainable. For instance, in the problem considered in [26] the authors computed, for an assumed frequency of 25 Hz, eight wavenumbers, implying eight dispersion curves. When the acoustic boundary problems of sandwich, infinite panels are considered, within the frequency range 16–20000 Hz, we usually need to obtain much less coincidence frequencies and dispersion curves.

The analysis in [8], made within the simplified model for a three-layer sandwich panel, shows formally the existence of three dispersion curves, i.e., three kinds of waves appearing in the structure. Since one of the waves is the evanescent one whereas the other may be propagating or evanescent (depending on frequency), hence only one kind of the waves and one dispersion curve is of practical importance. This is the so-called in-phase flexural wave. The facts established in [8] are convergent with results in [27], obtained from investigation of a more advanced model for the three-layer, thick sandwich plate.

It is seen from [27] that for the acoustic problems of the three-layer symmetric, thick sandwich plates, two kinds of propagating waves are primarily important; that is, the in-phase waves (considered in [8]) and the anti-phase, out-of-plane (so-called breathing) waves. The opinion is confirmed in [9] where the Author, considering only the in-phase and anti-phase waves, came to the following conclusion: when a sandwich plate has a set of parameters typical for the naval and aerospace applications, then the elementary theories predict wave motions of the plate in the whole frequency range of practical interest.

In the present paper, the coincidence frequencies have been obtained for the in-phase and anti-phase waves propagating in three-layer and five-layer panels, whereas the dispersion curve for the in-phase waves propagating in the three-layer panel.

Computations of the coincidence frequencies or the wavenumbers, in a general case, consist of two steps. First, the algorithms based on the residue theorem (so-called winding integral techniques) are usually applied to compute the number of zeros of the function $F(\omega_g, k_s(\omega_g))$ within an assumed (sub)domain. Then the iteration algorithms are used to obtain the zeros. Some details on the advanced computations of the roots are given, e.g. in [26]. For the sandwich structures one can apply a less refined way to find out zeros of the function, depending on the available software. In particular, the first step can be modified due to prompts from the literature as for instance [8].

6. Numerical results

In order to show a broad applicability of the local model proposed in the paper, both the critical coincidence frequencies and the TL for homogeneous (one-layer) and for layered I-I panels were computed. The results have been compared, whenever it was possible, with their counterparts calculated according to another models existing in the literature. All the numerical results are presented in the Figs. 3–6, 8–11 and in the Tables 1–4.

Results presented in and Table 1 and Fig. 3 were obtained for a homogeneous I-I panel and the following input data: $h_{(1)} = 6.63$ mm, $E_{(1)} = 0.689 \cdot 10^{11}$ Pa,

Table 1. The flexural coincidence frequencis (Hz) of the homogeneous aluminium I-I plate.

θ	12	18	24	30	36	42	48	54
$(f_c)_{\mathrm{SK}}$	53921	21169	11692	7587.5	5433.7	4167.2	3365.4	2832.3
$(f_c)_{\mathrm{M}}$	52049	20812	11577	7537.5	5407.8	4151.9	3355.3	2825.1
Δ	3.60	1.72	0.99	0.66	0.48	0.37	0.30	0.25

θ	60	66	72	78	84	90
$(f_c)_{\mathrm{SK}}$	2467.3	2214.5	2041.6	1929.0	1865.4	1844.8
$(f_c)_{\mathrm{M}}$	2461.8	2210.1	2037.8	1925.6	1862.3	1841.8
Δ	0.22	0.20	0.19	0.18	0.17	0.16

$\nu_{(1)} = 0.33$, $\rho_{(1)} = 2700$ kg/m^3. Apart from $h_{(1)}$, these data are the material parameters of aluminium. It is noted that the (shear modulus)/density $\equiv (\mu_{(1)}/\rho_{(1)})$ ratio in the case equals $9.59 \cdot 10^6$.

It is seen from the data in Table 1 that the coincidence frequencies predicted by the present local model $(f_c)_{\mathrm{SK}}$ are higher than the corresponding coincidence frequencies $(f_c)_{\mathrm{M}}$ predicted by the Mindlin theory, and the percentage difference $\Delta = 100[(f_c)_{\mathrm{SK}} - (f_c)_{\mathrm{M}}]/(f_c)_{\mathrm{M}}$ is dependent on θ and it is higher for the smaller values of the incident angle θ.

The coincidence curves, $\omega_c/\omega_{cr} \equiv f_c/f_{cr}$, for the flexural waves in domain of the incident angle $\theta \equiv$ eta are presented in Fig. 3. The curve denoted SK

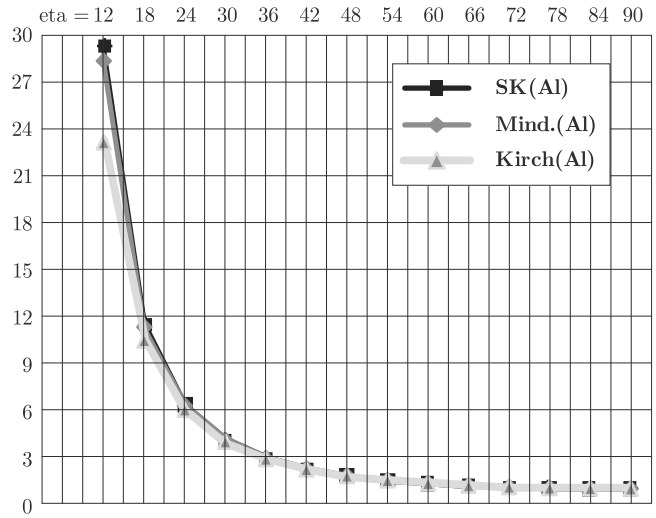

FIG. 3. The coincidence curves for the flexural waves in homogeneous aluminium panel.

results from the present local model, the curve denoted Mind. refers to the results predicted by the Mindlin type theory and the curve denoted Kirch refers to the results obtained according to the Kirchhoff theory.

It is interesting to note that the curves obtained according to the present local model and the Mindlin model are almost identical for the incident angle between 12 and 90 degrees, while the curve resulting from the Kirchhoff theory does not match with the SK and Mind curves for the incident angle between 12 and 24 degrees. It is noted however that the good agreement between the SK and Mind. curves in Fig. 3 does not imply a perfect agreement between the coincidence frequencies $(f_c)_{\mathrm{SK}}$ and $(f_c)_{\mathrm{M}}$ within the whole range of the incident angle – see Table 1.

Table 2. The flexural coincidence frequences (Hz) of the homogeneous I-I plaster board.

θ	42	48	54	60	66	72	78	84	90
$(f_c)_{\mathrm{SK}}$	19465	10496	7450.4	5897.4	4987.9	4426.9	4084.7	3898.8	3839.7
$(f_c)_{\mathrm{M}}$	17801	9437.9	6771.8	5416.3	4617.7	4121.6	3817.5	3651.6	3598.8
Δ	9.35	11.21	10.02	8.88	8.02	7.41	7.00	6.77	6.69

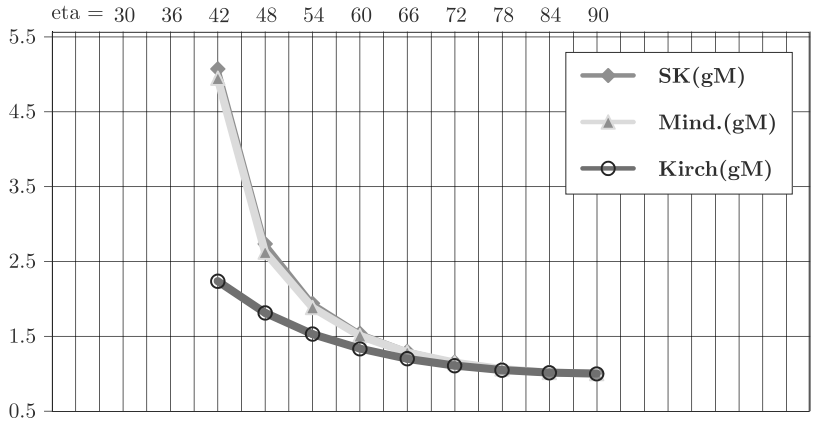

FIG. 4. The coincidence curves for the flexural waves in homogeneous gypsum board panel.

In Table 2 and Fig. 4 some results similar to those presented above are given. They were computed for a homogeneous I-I panel of the following parameters: $h_{(1)} = 25$ mm, $E_{(1)} = 0.1 \cdot 10^{10}$ Pa, $\nu_{(1)} = 0.16$, $\rho_{(1)} = 1200$ kg/m^3. These input data are approximately parameters of the gypsum board. Let us note that the (shear modulus)/density $\equiv (\mu_{(1)}/\rho_{(1)})$ ratio in the case equals $3.59 \cdot 10^5$. The ratio is 26.7 times lower than its counterpart in the previous example.

It is seen from the data in Table 2 that the coincidence frequencies predicted by the present local model $(f_c)_{\mathrm{SK}}$ are higher than the corresponding coincidence frequencies $(f_c)_{\mathrm{M}}$ predicted by the Mindlin-type theory and the percentage difference $\Delta = 100[(f_c)_{\mathrm{SK}} - (f_c)_{\mathrm{M}}]/(f_c)_{\mathrm{M}}$ is dependent on θ. Comparing the percentage differences $\Delta = 100[(f_c)_{\mathrm{SK}} - (f_c)_{\mathrm{M}}]/(f_c)_M$ from the Tables 1 and 2 one can see that accuracy of the Mindlin theory decreases with decreasing of the (shear modulus)/density ratio. Actually, for the aluminium panel the Δ does not exceed 0.4% within the range of the incident angle between 42 and 90 degrees, while for the plasterboard panel it is higher than 6.69%.

The coincidence curves, $\omega_c/\omega_{cr} \equiv f_c/f_{cr}$, in domain of the incident angle $\theta \equiv$ eta are shown in Fig. 4. It is seen that the curve resulting from the Kirchhoff theory is much below the other curves within the range of the incident angle between 42 and 72 degrees.

To complete discussion of the example, it is noted that the numerical analysis showed lack (absence) of the coincidence phenomenon in the panel for the incident angle less than 39 degrees. Within the range of the incident angle between 0 and 39 degrees solutions of the characteristic equation, of the eigenvalue problem, within the local model have not been detected, whereas frequencies resulting from the Mindlin wave equation have been imaginary numbers.

In Table 3 and Fig. 5 some numerical results for the classical three-layer sandwich I-I panel are presented for the following input data, given in [8]: $h_{(1)} = 0.5$ mm, $E_{(1)} = 0.3210^{11}$ Pa, $\nu_{(1)} = 0.3$, $\rho_{(1)} = 1264$ kg/m^3, $h_{(2)} = 10$ mm, $E_{(2)} = 0.5032 \cdot 10^9$ Pa, $\nu_{(2)} = 0.85$, $\rho_{(2)} = 137.6$ kg/m^3, $h_{(1)} = h_{(3)}$, $E_{(1)} = E_{(3)}$, $\nu_{(1)} = \nu_{(3)}$, $\rho_{(1)} = \rho_{(3)}$. It is explained that the isotropic middle layer with the Poisson ratio equal to 0.85 ($\nu_{(2)} = 0.85$) is an approximation of the honeycomb core considered in paper [8]. The Young's modulus $E_{(2)} = 2(1 + \nu_{(2)})G_e$, where G_e denotes the shear modulus given in [8]. The approximation, with Poisson's ratio of the honeycomb layer close to 1, has not been applied in [8] but it is well justified. It has been applied e.g. in [28]. The coincidence curve in Fig. 5 denoted by the abbreviation Mind.([8]) was obtained the same way as the corresponding curves in Figs. 3, 4 that is by applying the model called in [18] the Mindlin-type theory. The curve denoted by SK([8]) was obtained according to the local model presented in Sections 2–5.

Table 3. The flexural coincidence frequencis (Hz) of the three-layer I-I sandwich plate.

θ	30	36	42	48	54	60	66	72	78	84	90
$(f_c)_{\mathrm{SK}}$	7903.8	4046.0	2730.9	2063.1	1668.5	1416.8	1250.4	1139.8	1069.2	1029.8	1017.2
$(f_c)_{\mathrm{M}}$	9141.4	4327.9	2882.9	2167.3	1748.6	1482.9	1307.6	1191.4	1117.2	1075.9	1062.6
Δ	13.54	6.51	5.27	4.81	4.58	4.46	4.37	4.33	4.30	4.28	4.27

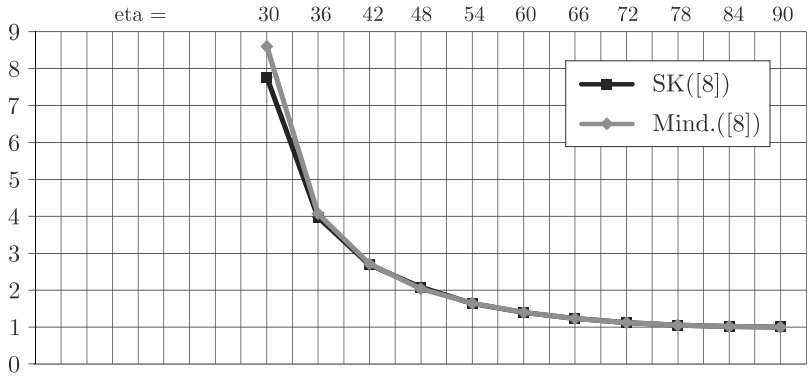

FIG. 5. The coincidence curves for the flexural waves in the three-layer sandwich panel investigated in [8].

Comparison of the percentage differences $\Delta = 100[(f_c)_{\mathrm{SK}} - (f_c)_{\mathrm{M}}]/(f_c)_{\mathrm{M}}$ listed in Table 3 enables us to conclude that accuracy of the coincidence frequency predicted by the Mindlin-type theory [18] decreases with decreasing the incident angle (it is also seen in Fig. 5.). The numerical analysis in this case showed lack of the the coincidence phenomenon in the three-layer sandwich panel for the incident angle less than 27 degrees. Within the range of the incident angle between 0 and 27 degrees, solutions of the characteristic equation, of the eigenvalue problem, within the local model have not been detected, whereas frequencies resulting from the Mindlin-type wave equation are found to be imaginary numbers.

In Figure 6 and Table 4 some nummerical results for a five-layer sandwich I-I panel are presented. Parameters of the structure are as follows: $h_{(1)} = 1$ mm, $E_{(1)} = 0.68910^{11}$ Pa, $\nu_{(1)} = 0.276$, $\rho_{(1)} = 2680$ kg/m^3, $h_{(2)} = 0.75$ mm, $E_{(2)} = 0.39 \cdot 10^{10}$ Pa, $\nu_{(2)} = 0.08$, $\rho_{(2)} = 1175$ kg/m^3, $h_{(3)} = 61.5$ mm, $E_{(3)} = 0.3059 \cdot 10^9$ Pa, $\nu_{(3)} = 0.85$, $\rho_{(3)} = 32.8$ kg/m^3, $h_{(2)} = h_{(4)}$, $E_{(2)} = E_{(4)}$, $\nu_{(2)} = \nu_{(4)}$,

Table 4. The flexural and breathing coincidence frequencies (Hz) of the five-layer I-I sandwich plate.

θ	12	18	24	30	36	42	48	54
$(f_{\mathrm{cF}})_{\mathrm{SK}}$	52063	11083	3141.2	997.3	561.6	388.0	296.1	240.7
$(f_{\mathrm{cB}})_{\mathrm{SK}}$						25379	20566	17477

θ	60	66	72	78	84	90
$(f_{\mathrm{cF}})_{\mathrm{SK}}$	205.1	181.3	165.5	155.4	149.7	147.9
$(f_{\mathrm{cB}})_{\mathrm{SK}}$	15421	14026	13085	12479	12139	12029

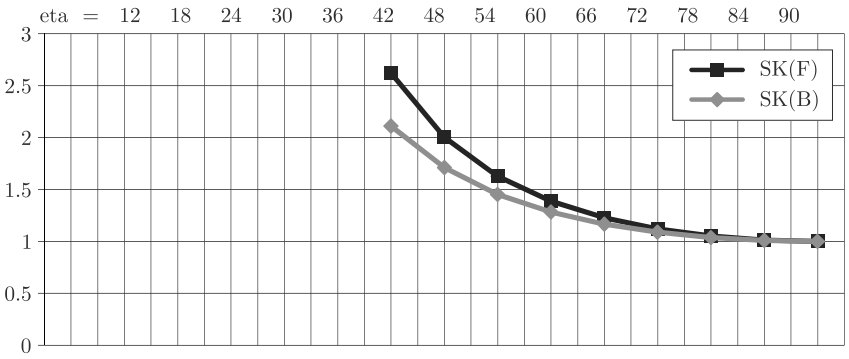

FIG. 6. The coincidence curves for the flexural and breathing waves in the five-layer sandwich panel.

$\rho_{(2)} = \rho_{(4)}$, $h_{(1)} = h_{(5)}$, $E_{(1)} = E_{(5)}$, $\nu_{(1)} = \nu_{(5)}$, $\rho_{(1)} = \rho_{(5)}$. The layers 2, 4 may be for instance of the glue necessary to connect the outer aluminium layers and the middle honeycomb core. Thicknesses of the layers 2 and 4 are 50% higher than the values given in [4]. (As in the previous example, the isotropic middle layer with the Poisson ratio equal to 0.85 ($\nu_{(3)} = 0.85$) is an approximation of the honeycomb core). Unfortunately, the results, presented in Fig. 6 and Table 4, are not compared since the author did not find in the literature experimental or numerical data being appropriate for the comparison.

The curve SK(F) in Fig. 6 denotes the coincidence curve, $\omega_c/\omega_{cr} \equiv f_c/f_{cr}$, in domain of the incident angle $\theta \equiv$ eta for the flexural waves and the curve SK(B) is the ratio in domain of the incident angle for the breathing waves propagating in the five-layer structure.

In Table 4 the symbol with subscript F denotes coincidence frequencies for the flexural waves, whereas symbol with subscript B denotes coincidence frequencies for the breathing waves.

It is explained that the breathing coincidence frequencies for the incident angle less than 42 degrees have not been detected. Looking at the results in Table 4 one can see that the sound insulation by means of the five-layer structure would be inefficient in the range of low frequencies, because of the 'flexural' coincidence phenomenon, and in the range of very high frequencies because of the breathing waves propagating in the core and the associated 'breathing' coincidence phenomenon.

In order to show a versatility of the local model, a second, non-classical, three-layer sandwich panel has been investigated. The structure is composed of two thick outer layers (gypsum boards) and of thin, more compliant middle layer. The computations were made for the following input data: $h_{(1)} = 12.5$ mm, $E_{(1)} = 0.2 \cdot 10^{10}$ Pa, $\nu_{(1)} = 0.2$, $\rho_{(1)} = 1200$ kg/m^3, $h_{(2)} = 2$ mm, $E_{(2)} = 0.925 \cdot 10^7$ Pa, $\nu_{(2)} = 0.25$, $\rho_{(2)} = 92.5$ kg/m^3, $h_{(1)} = h_{(3)}$, $E_{(1)} = E_{(3)}$, $\nu_{(1)} = \nu_{(3)}$,

$\rho_{(1)} = \rho_{(3)}$. Cross-section of the structure is shown in Fig. 7. The parameter $E_{(2)} = 0.925 \cdot 10^7$ Pa is the Young's modulus for cork, however the computations presented below were done for different values of the parameter.

An influence of the Young's modulus of the middle layer on the critical coincidence frequency of the structure shown in Fig. 7 has been investigated. The results are presented in Fig. 8. On the vertical axis the values $f_{cr}/1000 = \omega_{cr}/(2\pi \cdot 1000)$ are marked, where $f_{cr} = \omega_{cr}/2\pi$ denotes the critical coincidence frequencies (Hz). On the horizontal axis the values $E_{(2)}/10^7$ (Pa) are denoted.

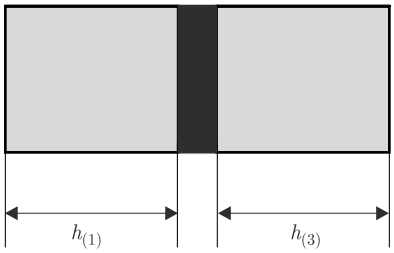

FIG. 7. Cross-section of the non-classical, sandwich panel composed of gypsum boards and cork.

It is seen in Fig. 8 that decreasing of the Young's modulus of the structure shown in Fig. 7 implies increasing of the critical coincidence frequency. For example, coordinates of the left-hand side point of the curve are $(0.925, 4.342)$, while coordinates of the right-hand side point of the curve are $(200, 2.106)$. The latter point refers to the homogeneous plate 27 mm thick.

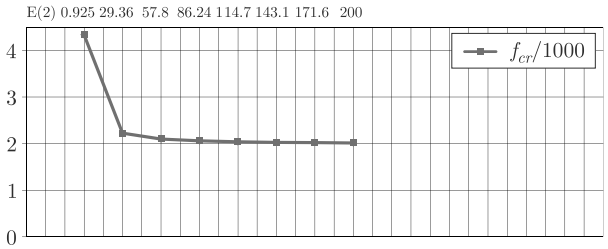

FIG. 8. Influence of the Young's modulus of the middle layer on the critical coincidence frequencies of the non-classical sandwich panel.

In order to test better the local model, the TL for homogeneous, aluminium, the purely elastic I-I plate of thickness 6.63 mm is presented. The computations were made following the idea outlined in the Appendix B for both the local model and the Kirchhoff model. Results in Fig. 9 are predicted by the Kirchhoff

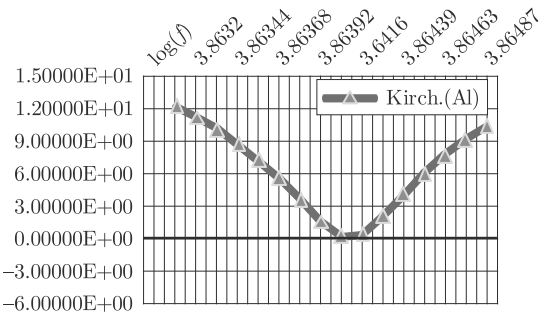

FIG. 9. The TL curve in vicinity of the coincidence frequencies for homogeneous plate, predicted by the Kirchhoff (Kirch.) model.

model. The curve has been obtained for the incident angle $\theta = 30^\circ$ in vicinity of the coincidence frequency for the model.

It was found from the curve (for the Kirchhoff model) that $\log_{10}(f_c) \approx 3.8641$ and $f_c \approx 7312.8$ Hz. For the exact local model, the corresponding values obtained from the TL computations are as follows: $\log_{10}(f_c) \approx 3.8801$ and $f_c \approx 7587.5$ Hz. These results, obtained from the TL computations, confirm the results presented in Table 1 and in Figs. 3, 4.

Finally, to make more extended analysis of the local model another two curves are presented for the three-layer sandwich structure discussed above. Dependence of the wavenumber k_s for the "in-phase" (flexural) waves on the frequency f (Hz) is shown in Fig. 10 within a wide range of frequency, i.e. from 10 untill 315000 Hz.

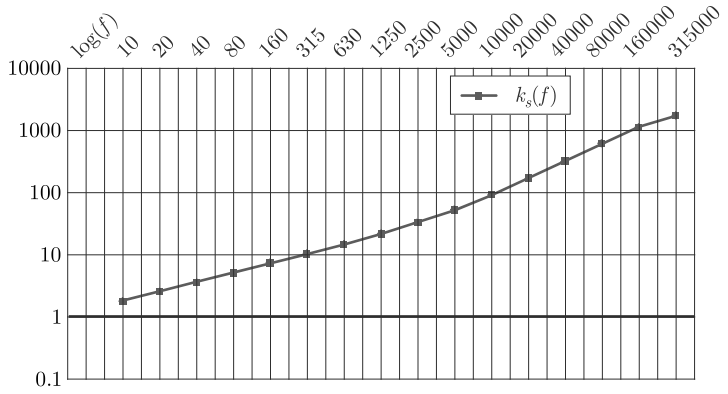

FIG. 10. Dependence of the wavenumber k_s on frequency f for the "in-phase" waves propagating in the three-layer sandwich structure.

In Fig. 11 the phase velocity cs of the "in-phase" wave in domain of the wavenumber k_s for the three-layer sandwich infinite panel is shown.

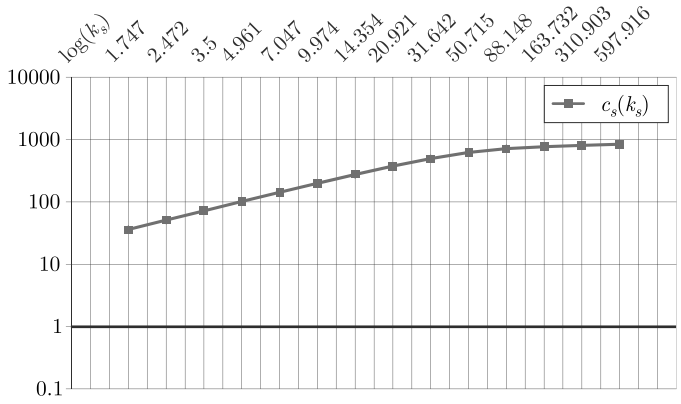

FIG. 11. Phase velocity c_s of the "in-phase" wave in domain of the wavenumber k_s, for the three-layer sandwich structure.

Let us note that shapes of the curves presented in Figs. 10 and 11 agree with expectations and with predictions existing in the literature. In particular, one may expect that the local model is stable in the sense pointed out in [20].

7. Conclusions

Local model of the plane acoustic waves propagation in multilayered infinite plate has been derived within the theory of linear elastodynamics. It is composed of two Lamé's rotational functions and of the volumetric function and finally, obtained with application of the Pythagorean theorem. It has been shown that the model corresponds to the benchmark plate model of LEVINSON [25].

The present local model is derived without any simplifications concerning the structure and therefore it predicts accurate results for homogeneous and multilayered plates including the sandwich structures composed of alternately arranged thin/thick stiff and thick/thin soft layers. In particular, both the flexural and breathing waves occurring in the sandwich structures are included. For the infinite-infinite (I-I) structures, forced by the plane waves, the model reduces to the 2D counterpart existing in the literature.

The numerical analysis shows that the Kirchhoff model and the Mindlin-type model do not predict the coincidence frequencies accurately, however the coincidence curves, defined in the Appendix A, predicted by the Mindlin-type model, are very close to the coincidence curves predicted by the local model. When a homogeneous plate is considered, accuracy of the Mindlin-type theory decreases with decreasing of the (shear modulus)/density ratio.

Numerical results show that the five-layer sandwich panels may not be good for the insulation purposes within the range of high frequencies because of the

breathing waves and the associated breathing coincidence phenomenon. The analysis of non-classical sandwich structure shows that a thin compliant layer placed between stiff thick layers increases significantly the critical coincidence frequency of the structure.

The TL computations in vicinity of the coincidence frequency confirm the conclusions resulting from the analysis of the coincidence phenomenon.

The curves $k_s(f)$ and $c_s(k_s)$ enable us to conclude that the local model is stable in the sense pointed out in [20].

Appendix A. Fundamental knowledge on the coincidence frequencies

The coincidence phenomenon in a structure is commented by means of Fig. 12. Symbols λ_A, λ_S denote length of the incident wave (in the air) and wave propagating in the structure, respectively.

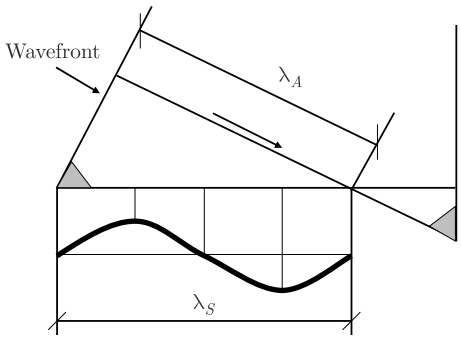

FIG. 12. The coincidence phenomenon.

Occurrence of the coincidence phenomenon in I-I structure can shortly be noted as follows [17]

$$(\lambda_A/\sin\theta = \lambda_s \equiv c/\sin\theta = c_s) \;\Leftrightarrow\; \omega = \omega_c. \tag{A.1}$$

Symbols ω and ω_c in (A.1) denote frequency of the incident wave and the coincidence frequency of the structure, respectively. Symbols λ_s, c_s in the above relationship denote the length and velocity of the sound wave propagating in the structure, respectively. The velocities of the incident wave and the wave propagating in the structure can be expressed as follows [21],

$$\begin{aligned} &c = \lambda_A/T = \lambda_A f = \lambda_A\omega/2\pi = \omega/k, \\ &c_s = \omega/k_s, \qquad k = 2\pi/\lambda_A, \qquad k_s = 2\pi/\lambda_s, \end{aligned} \tag{A.2}$$

Directly from (A.1) one can write the following relationships

$$\omega_c = \eta(\theta), \qquad \theta \to 0 \;\Rightarrow\; c_s \to \infty \wedge \omega_c \to \infty. \tag{A.3}$$

The lowest coincidence frequency is called (in the literature) critical coincidence frequency and it occurs when the incident angle is equal to 90°, i.e.

$$\omega_{cr} = \eta(\theta = 90^\circ) = \omega_c(\theta = 90^\circ). \tag{A.4}$$

For a homogeneous panel, the left-hand side relationship in (A.3) can be expressed as follows [7],

$$\omega_c/\omega_{cr} = 1/\sin^2\theta. \tag{A.5}$$

In this paper the ratio ω_c/ω_{cr} is called 'coincidence curve'. The critical coincidence frequency ω_{cr} is of special importance because of the following reasons [17]. First, the critical coincidence frequency is the only coincidence frequency at which the TL of a F-F purely elastic plate equals zero. Second, the critical coincidence frequency of the F-F plate is independent of the incident angle θ. Third, the critical coincidence frequency of the F-F plate equals the critical coincidence frequency of the I-I panel, with the same cross-sectional parameters as the F-F plate. The third property can be noted in the following form:

$$(\omega_{cr})_{I-I} = (\omega_{cr})_{F-F}. \tag{A.6}$$

Due to the third property, the critical coincidence frequency can be calculated either within models (theories) for the F-F plates or within the corresponding models for the I-I panels.

Appendix B. Details on computation of the TL

Definition of the TL for an assumed incident angle θ is as follows:

$$TL_\theta = 10\log_{10}(1/\tau_\theta) = 10\log_{10}|p_i/p_t|^2. \tag{B.1}$$

Directly from (B.1) one obtains the following relationship:

$$p_t = \pm p_i \;\Leftrightarrow\; TL_\theta = 10\log_{10}|p_i/p_t|^2 = 0. \tag{B.2}$$

In order to obtain the average value of the TL, the following formula is given in the literature,

$$TL = 10\log_{10}\left(\int_0^{\theta_1}\cos\theta\sin\theta d\theta \Big/ \int_0^{\theta_1}\tau_\theta\cos\theta\sin\theta d\theta\right) = 0. \tag{B.3}$$

The θ_1 is usually assumed as equal 78°.

References

1. M.D. RAO, *Recent applications of viscoelastic damping for noise control in automobiles and commercial airplanes*, Journal of Sound and Vibration, **262**, 457–474, 2003.
2. C. GRIMWOOD, *Complaints about poor sound insulation between dwellings in England and Wales*, Applied Acoustics, **52**, 211–223, 1997.
3. X. WANG, A. STARLINGER, R.J. DEAN, J. WIESCHERMANNK, *The application of sandwich components in the design of the new transrapid maglev TR08 vehicles*, Proceedings of the 5th International Conference on Sandwich Construction, Vol. 2, 539–549, ETH Zurich, Switzerland, September 2000.
4. S.W. BOYD, J.I. BLAKE, R.A. SHENOI, J. MAWELLA, *Optimisation of steel-composite connections for structural marine applications*, Composites: Part B, **39**, 891–906, 2008.
5. A.S. HERRMANN, P.C. ZAHLEN I. ZUARDY, *Sandwich structures technology in commercial aviation*, Proceedings of the 7th International Conference on Sandwich Construction, 13–26, Aalborg University, Denmark, August 2005.
6. T. MATSUMOTO, M. UCHIDA, H. SUGAYA, H. TACHIBANA, *Development of multiple drywall with high sound insulation performance*, Applied Acoustics, **67**, 595–608, 2006.
7. K. RENJI, *Sound transmission loss of unbounded panels in bending vibration considering transverse shear deformation*, Journal of Sound and Vibration, **283**, 478–486, 2005.
8. E. NILSSON, A.C. NILSSON, *Prediction and measurement of some dynamic properties of sandwich structures with honeycomb and foam cores*, Journal of Sound and Vibration, **251**, 409–430, 2002.
9. S.V. SOROKIN, *Analysis of wave propagation in sandwich plates with and without heavy fluid loading*, Journal of Sound and Vibration, **271**, 1039–1062, 2004.
10. S.V. SOROKIN, N. PEAKE, *On symmetry-breaking effects in propagation of waves in sandwich plates with and without heavy fluid loading*, Journal of Sound and Vibration, **295**, 114–128, 2006.
11. P. THAMBURAJ, J.Q. SUN, *Effect of material and geometry on the sound and vibration transmission across a sandwich beam*, ASME Journal of Vibration and Acoustics, **123**, 205–212, 2001.
12. P. THAMBURAJ, J.Q. SUN, *Effect of material anisotropy on the sound and vibration transmission loss of sandwich aircraft structures*, Journal of Sandwich Structures and Materials, **1**, 76–92, 1999.
13. T. WANG, V.S. SOKOLINSKY, S. RAJARAM, S.R. NUTT, *Assessment of sandwich models for the prediction of sound transmission loss in unidirectional sandwich panels*, Applied Acoustics, **66**, 245–262, 2005.
14. J.A. MOORE, *Sound transmission loss characteristics of three-layer composite wall constructions*. Ph.D. thesis, MIT, 1975.
15. A.E. JENSEN, A.F. INGENS, *Thickness vibrations of sandwich plates and beams and delamination detection*, Journal of Intelligent Material Systems and Structures, **10**, 1999.
16. R. ZHOU, M.J. CROCKER, *Sound transmission loss of foam-filled honeycomb sandwich panels using statistical energy analysis and theoretical and measured dynamic properties*, Journal of Sound and Vibration, **329**, 673–686, 2010.

17. M.C. BHATTACHARYA, R.W. GUY, M.J. CROCKER, *Coincidence effect with sound waves in a finite plate*, Journal of Sound and Vibration, **18**, 157–169, 1971.

18. K. RENJI, P.S. NAIR, S. NARAYANAN, *Critical and coincidence frequencies of flat panels*, Journal of Sound and Vibration, **205**, 19–32, 1997.

19. R.M. JONES, *Mechanics of Composite Materials*, McGraw-Hill, New York 1975.

20. A.V. METRIKINE, *On casuality of the gradient elasticity models*, Journal of Sound and Vibration, **297**, 727–742, 2006.

21. A. PAOLOZZI, I. PERONI, *Response of aerospace sandwich panels to launch acoustic environment*, Journal of Sound and Vibration, **196**, 1–18, 1996.

22. J. SZYMCZYK, CZ. WOŹNIAK, *Continuum modeling of laminates with slowly graded microstructure*, Archives of Mechanics, **58**, 445–448, 2006.

23. J.D. ACHENBACH, *Wave Propagation in Elastic Solids*, North-Holland Publishing Company, Amsterdam, New York, Oxford 1973.

24. J. MIKLOVITZ, *The Theory of Elastic Waves and Waveguides*, North-Holland Publishing Company, Amsterdam, New York, Oxford 1978.

25. M. LEVINSON, *Free vibrations of a simply supported rectangular plate: an exact three-dimensional linear elasticity solution*, Journal of Sound and Vibration, **15**, 283–291, 1985.

26. S. IVANSSON, I. KARASALO, *Computation of wavenumbers using an adaptive winding-number integral method with error control*, Journal of Sound and Vibration, **161**, 173–180, 1993.

27. A.C. NILSSON, *Wave propagation in and sound transmission through sandwich plates*, Journal of Sound and Vibration, **138**, 73–94, 1990.

28. C.W. BERT, D.J. WILKINS JR., W.C. CRISMAN, *Damping in sandwich beams with shear flexible cores*, ASME Journal of Engineering for Industry, **89**, 662–670, 1967.

Received December 31, 2010; revised version October 17, 2011.